Journal of Vacuum Science and Technology B

RESEARCH ARTICLE | MARCH 27 2024

Temperature-dependent morphology and composition of ultra-thin GeSn epilayers prepared by remote plasma enhanced chemical vapor deposition

Jiechao Jiang ; Nonso Martin Chetuya; Efstathios I. Meletis; Joseph H. Ngai; Gordon J. Grzybowski ; Bruce Claflin

Check for updates

J. Vac. Sci. Technol. B 42, 034001 (2024)
https://doi.org/10.1116/6.0003445

View Online
Export Citation

27 March 2024 13:52:56

JVST B
Journal of Vacuum Science & Technology B

ARTICLE

pubs.aip.org/avs/jvb

Temperature-dependent morphology and composition of ultra-thin GeSn epilayers prepared by remote plasma enhanced chemical vapor deposition

Cite as: J. Vac. Sci. Technol. B 42, 034001 (2024); doi: 10.1116/6.0003445
Submitted: 10 January 2024 · Accepted: 7 March 2024 ·
Published Online: 27 March 2024

View Online Export Citation CrossMark

Jiechao Jiang,[1,a)] Nonso Martin Chetuya,[1] Efstathios I. Meletis,[1] Joseph H. Ngai,[2] Gordon J. Grzybowski,[3] and Bruce Claflin[4]

AFFILIATIONS

[1]Materials Science and Engineering Department, University of Texas at Arlington, Arlington, Texas 76019
[2]Department of Physics, University of Texas at Arlington, Arlington, Texas 76019
[3]KBR, 3725 Pentagon Blvd., Suite 100, Beavercreek, Ohio 45431
[4]Air Force Research Laboratory, 2241 Avionics Circle, Wright-Patterson, AFB, Ohio 45433

Note: This paper is part of the 2024 Special Topic Collection on Developing SiGeSn Technology: Materials and Devices.
[a)]**Electronic mail:** jiangjc@uta.edu

27 March 2024 13:52:56

ABSTRACT

Two distinct ultra-thin $Ge_{1-x}Sn_x$ ($x \leq 0.1$) epilayers were deposited on (001) Si substrates at 457 and 313 °C through remote plasma-enhanced chemical vapor deposition. These films are considered potential initiation layers for synthesizing thick epitaxial GeSn films. The GeSn film deposited at 313 °C has a thickness of 10 nm and exhibits a highly epitaxial continuous structure with its lattice being compressed along the interface plane to coherently match Si without mismatch dislocations. The GeSn film deposited at 457 °C exhibits a discrete epitaxial island-like morphology with a peak height of ~30 nm and full-width half maximum (FWHM) varying from 20 to 100 nm. GeSn islands with an FWHM smaller than 20 nm are defect free, whereas those exceeding 25 nm encompass nanotwins and/or stacking faults. The GeSn islands form two-dimensional modulated superlattice structures at the interface with Si. The GeSn film deposited at 457 °C possesses a lower Sn content compared to the one deposited at lower temperature. The potential impact of using these two distinct ultra-thin layers as initiation layers for the direct growth of thicker GeSn epitaxial films on (001) Si substrates is discussed.

Published under an exclusive license by the AVS. https://doi.org/10.1116/6.0003445

I. INTRODUCTION

High-quality epitaxial GeSn films with Sn content exceeding 6 at. %, offer exceptionally promising electrical and optical properties needed for applications spanning near- and mid-infrared detectors, emitters, and lasers.[1–7] However, the inherent challenges with these alloys, including the limited bulk solubility of Sn in Ge,[8] the propensity for Sn to segregate or precipitate from GeSn at elevated temperatures, and the substantial lattice mismatch between GeSn films and Si substrates, present considerable obstacles in achieving epitaxial GeSn films of superior quality. To surmount these challenges and attain higher Sn content in GeSn films, significant recent efforts have been directed toward innovating diverse techniques using low-temperature, non-equilibrium growth processes. One example among these methods is remote plasma-enhanced chemical vapor deposition (RPECVD), which provides the capability for fast growth of epitaxial GeSn films.[9,10]

Another challenge in achieving high-quality epitaxial GeSn thin films with a high Sn content on (001) Si is the substantial lattice mismatch between the film and the substrate. Such a large lattice mismatch at the interface produces compressive strain in the film, leading to structural defects such as edge or threading dislocations. To address this challenge, methods such as introduction of an intermediate Ge buffer layer (sometimes called a Ge virtual substrate) or a graded buffer layer prior to GeSn film growth have been

Published under an exclusive license by the AVS

employed. The goal of such buffer layers is to reduce the strain and enhance film quality by minimizing the occurrence of defects.[11–15] In this work, we report on a comprehensive examination of the morphology, composition, and microstructure of two ultra-thin GeSn layers on (001) Si that can potentially be used as initiation layers for deposition of thick epitaxial GeSn films directly on Si without any buffer layer. These nucleation layers were deposited by RPECVD at two distinct temperatures to better understand the growth temperature-composition-microstructure-strain relaxation relationship near the interface.

II. EXPERIMENT

Two distinct $Ge_{1-x}Sn_x$ ($x \leq 0.1$) ultra-thin initiation layers were deposited via RPECVD at a high temperature of 457 °C (denoted as HTIL) and a standard temperature of 313 °C (denoted as STIL), respectively. The layers were grown using 42 SCCM flows of 6% GeH_4/He and 12.5 SCCM of $SnCl_4$/He with an additional 3.75 SCCM He dilution. For substrate preparation, the (001) Si substrates were etched for 1 min in a dilute HF solution to eliminate the native oxide layer prior to being introduced into the growth apparatus. The deposition time for both initiation layers was 45 s. Further details of the growth process and equipment configuration have been reported previously.[9,10]

The surface composition of the films was investigated by x-ray photoelectron spectroscopy (XPS) conducted in a Perkin-Elmer Phi 560 ESCA/SAM system using an Al K_α excitation source (1484.6 eV). Survey spectra spanning the range 0–1300 eV were acquired with a step size of 0.2 eV and a pass energy of 100 eV. Calibration of binding energy (BE) relied on the C 1s peak, positioned at 284.8 eV. Raman spectra were captured using a ThermoFisher DXR3 Raman microscope with a 532 nm laser. To assess surface morphology, scanning electron microscopy (SEM) was conducted using a Hitachi S-4800 field-emission microscope equipped with an EDAX energy-dispersive spectroscopy (EDS) system, operating at 3 keV and atomic force microscopy (AFM) was conducted using a Park XE 70 AFM. Cross-sectional and plan-view specimens were prepared for transmission electron microscopy (TEM) through mechanical grinding, polishing, and dimpling using a Gatan Model 656 dimple grinder. Subsequent Ar-ion milling was performed in a Gatan Model 691 precision ion polishing system. The intricate microstructure of the films was explored in depth using a Hitachi H-9500 high-resolution (HR) transmission electron microscope operating at 300 keV. The microscope, with a lattice resolution of 0.10 nm, was equipped with an EDAX EDS system.

III. RESULTS AND DISCUSSION

The surface morphology and roughness of ultra-thin GeSn HTIL and STIL were investigated using SEM and AFM in non-contact mode with a $1 \times 1\,\mu m^2$ scanned area. Figures 1(a) and 1(c) display an SEM image and an AFM image, respectively, illustrating the surface morphology of the ultra-thin GeSn HTIL. The SEM image resembles the characteristics of a rock garden floor, while the AFM image reveals a rough island structure. The structures in this film have sizes ranging from 20 to 150 nm in diameter with an average mean roughness (Ra) of 3.53 nm. Figures 1(b) and 1(d) show similar SEM and AFM images, respectively, of the GeSn STIL, revealing the surface morphology of the ultra-thin GeSn STIL. Both STIL images exhibit a significantly smoother surface compared to the HTIL, with a Ra value of 0.27 nm.

We investigated the surface composition of GeSn HTIL and STIL using XPS, Fig. 1(f). The Sn content in the HTIL and STIL films is ~6.0 and ~9.5 at. %, respectively.

We also examined the GeSn HTIL and STIL using Raman spectroscopy, Fig. 1(e). The GeSn HTIL and STIL films exhibit a peak at 296.0 and 291.5 cm^{-1}, respectively. The Sn content estimated from the Ge–Ge vibration mode peak position is ~6.5% for the HTIL and ~12.5% for the STIL films using the compositional dependence of the Ge–Ge mode position in GeSn alloys reported in the literature.[16]

Figure 2(a) shows a cross-sectional TEM image of the GeSn HTIL film on Si taken with the electron beam parallel to the Si [110] direction, clearly revealing a discrete island-like morphology within the film. The peak height of the islands is about 28 nm, with the base of the islands situated on the Si substrate. The islands exhibit a lateral full-width at half maximum (FWHM) that ranges from 30 to 100 nm, with distances between islands (the thickness of the boundaries between them) ranging from 4 to 15 nm. Selected area electron diffraction (SAED) pattern studies show that the distinct islands all share the same crystallographic orientation.

Figure 2(b) shows an SAED pattern taken from a region encompassing multiple islands within the GeSn HTIL film and Si presenting a clean superposition pattern of [110] Si and [110] GeSn. This observation indicates formation of highly epitaxial GeSn islands on Si. The GeSn islands have an orientation relationship of $(001)_{GeSn}//(001)Si$, $[100]_{GeSn}//[100]_{Si}$, $[010]_{GeSn}//[010]_{Si}$, and lattice mismatches of 5.2% along the interface direction and 4.7% along the vertical direction, with respect to the Si substrate.

The GeSn island morphology and distribution in the film plane were studied through plan-view TEM. Figure 2(c) shows a plan-view TEM image of GeSn HTIL/Si obtained by removing the substrate using ion milling, demonstrating a pattern composed of distorted, non-specific shapes. The bright boundaries in Fig. 2(c) correspond to areas where Si from the substrate is present without the presence of GeSn structures, whereas the dark domains enclosed by the white boundaries are indicative of GeSn structures, consistent with the island formations shown in Fig. 2(a). The dark domains have a width ranging from 20 to 100 nm, while the white boundaries measure between 10 and 20 nm. Figure 2(d) shows one-quarter of an SAED pattern extracted from a plan-view sample of the GeSn HTIL/Si interface. In this case, the electron beam was aligned parallel to the [001] axis of the Si substrate. Figure 2(d) was taken from a region encompassing many dark domains in Fig. 2(c). The pattern displays a clean and well-defined superposition of the [001] Si and [001] GeSn patterns serving as a further strong indicator of the highly epitaxial nature of the GeSn islands on the Si substrate. The lattice mismatch measured in the SAED pattern from the plan-view sample [Fig. 2(d)] is 5.20%, the same as the value measured from the cross-sectional TEM sample [Fig. 2(b)]. The Sn content in the GeSn islands can be approximately determined to be 7 at. % obtained by using the formula $x = (a_{exp} - a_{Ge})/(a_{Sn} - a_{Ge})$, where a_{exp} is the lattice constant measured from the SAED pattern and a_{Sn} and a_{Ge} correspond to the lattice constant of α-Sn and Ge, respectively. EDS analysis, performed using an electron beam with a 10 nm diameter probe, reveals that the core area within a single

27 March 2024 13:52:56

Published under an exclusive license by the AVS

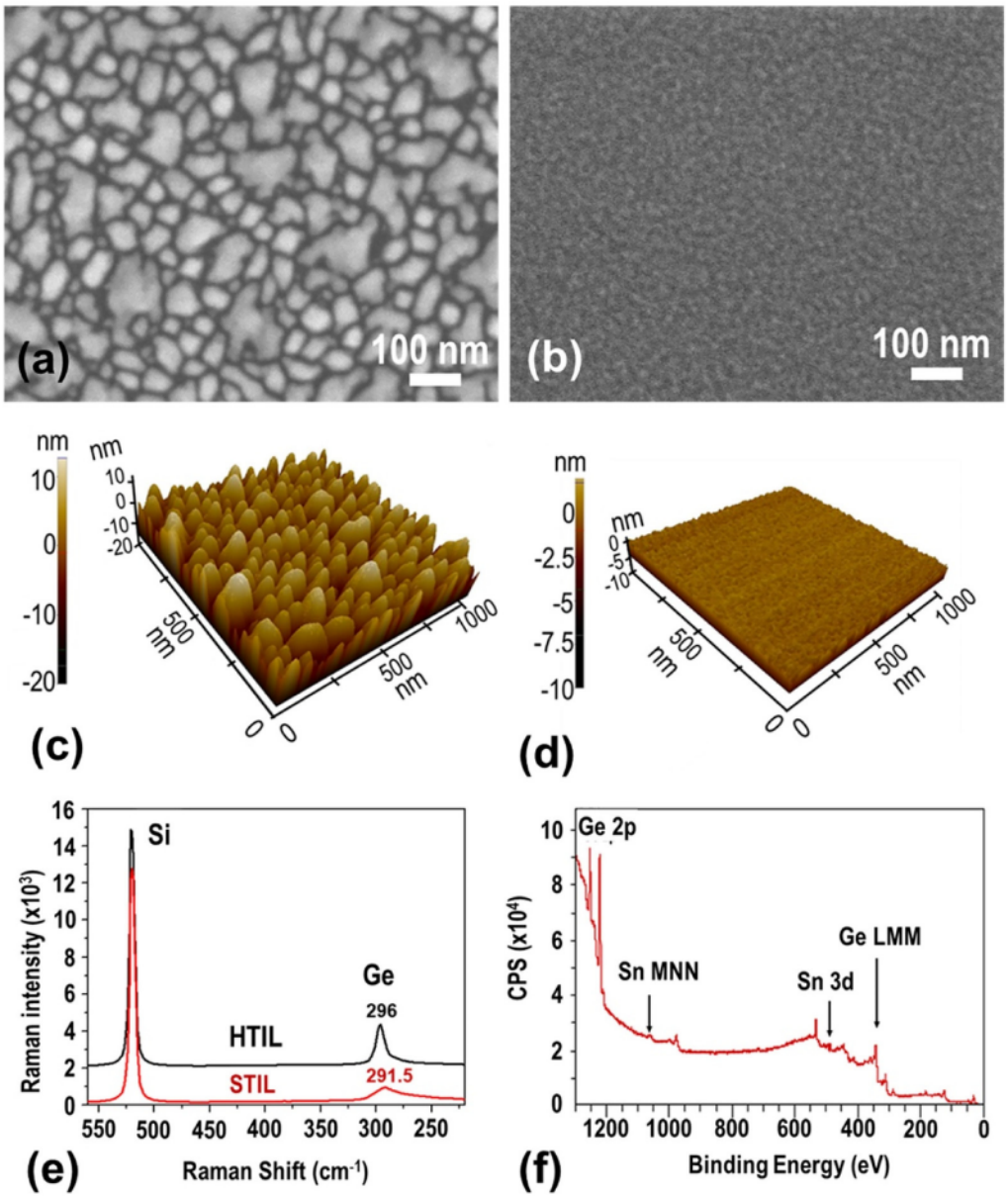

FIG. 1. (a), (c) and (b), (d) SEM and AFM images for HTIL and STIL films, respectively; (e) Raman spectra of GeSn HTIL and STIL on Si substrates, (f) XPS survey spectrum of GeSn STIL film.

island [refer to the core location in Fig. 2(a)] exhibits a somewhat lower Sn content of 7–8 at. % [as shown in the top spectrum in Fig. 2(e)] compared to the near-surface region of the island [refer to the surface region location in Fig. 2(a)], which has 9–10 at. % Sn [as depicted in the bottom spectrum of Fig. 2(e)].

In Figs. 3(a) and 3(b), cross-sectional HRTEM images of the GeSn HTIL/Si interface show the atomic structure of two distinct GeSn island-like structures with different sizes. The smaller, pyramid-like GeSn structure, measuring 20 nm in height and with an FWHM of 20 nm, presents itself as a defect-free structure above the interface, Fig. 3(a). Within this structure, three misfit dislocations (indicated by arrows) have formed at the interface with the substrate. The areas outside the pyramid-like GeSn structure appear as open spaces, exposing the Si substrate. Conversely, within the larger hill-like structures, characterized by an FWHM exceeding 25 nm, a few nanotwin structures were observed [see Fig. 3(b)].

27 March 2024 13:52:56

Published under an exclusive license by the AVS

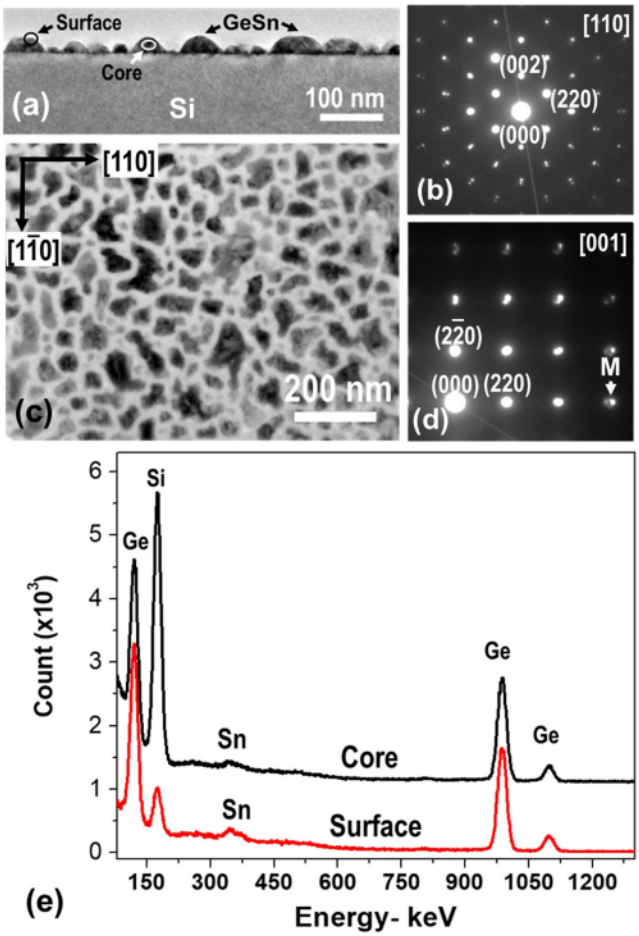

FIG. 2. (a) XTEM image and (b) SAED pattern of GeSn HTIL film on Si substrates, (c), (d) plan-view TEM image and one-quarter of a SAED pattern of the GeSn HTIL film on Si. (e) EDS spectra from the core and the near-surface regions as depicted in (a). Spot "M" in (d) is used for lattice misfit determination.

Figure 3(c) exhibits a magnified TEM image extracted from a plan-view sample of the GeSn HTIL/Si, with the electron beam aligned parallel to the Si [001] axis. This image shows well-defined, two-dimensional (2D), modulated superlattice arrangements within the GeSn domain regions, reminiscent of the patterns observed in HRTEM images in our previous studies of epitaxial films.[17–19] This modulation arises from the overlap of materials GeSn and Si at their interface. In contrast, the boundary bands, which have a width of approximately 10 nm, lack this modulated structure and are associated with GeSn-free regions.

Figure 3(d) exhibits an HRTEM image of a plan-view GeSn HTIL/Si revealing a periodic arrangement of finely distributed superlattices in the GeSn/Si region and Si lattices in the boundary band. The spacing of the lattice fringes, which corresponds to the modulation wavelength, measures approximately 38 Å along both the [110] and [1$\bar{1}$0] directions. This spacing signifies the coherent joining of the (110) planes of materials GeSn and Si at the interface every 38 Å, as schematically illustrated in Fig. 3(e). To accommodate the misfit strain between the two materials, a misfit dislocation emerges every 38 Å. The density of misfit dislocations at the HTIL/Si interface is $\sim 6.9 \times 10^{10}/\text{mm}^2$. The lattice spacing of the (220) plane in Si measures 1.92 Å. As a result, 20 (220) planes of Si [bottom left in Fig. 3(e)] align with 19 (220) planes of GeSn [top left in Fig. 3(e)] forming a superstructure with a lattice constant $a_s = 38$ Å [right in Fig. 3(e)]. In general, in a superstructure at the GeSn/Si interface, $n \times (220)_{\text{GeSn}}$ of the film matches $(n+1) \times (220)_{\text{Si}}$ of the substrate, and the lattice constant (a_s) of this superstructure can be calculated using the formula $a_s = n^* d^{\text{GeSn}}_{(220)} = (n+1)^* d^{\text{Si}}_{(220)}$. The lattice mismatch (δ) between the film and the substrate can be calculated using $\delta = (a_{\text{GeSn}} - a_{\text{Si}})/a_{\text{Si}} = ((a_s/n) - (a_s/n+1))/a_s/(n+1) = 1/n$. Since $n = 19$ in this case, the lattice mismatch at the interface is $1/19 = 5.26\%$, corresponding to a GeSn structure with a lattice constant of 5.717 Å. Estimations using the formula in the earlier section indicate a Sn content of approximately 7 at. % within the GeSn islands.

Figure 4(a) shows a cross-sectional TEM image of the GeSn STIL film on Si. In this image, the GeSn STIL presents a continuous layer with a flat and smooth surface and a sharp interface with Si. The GeSn STIL exhibits a thickness of 10.5 nm. Figure 4(b) presents an SAED pattern captured from the GeSn STIL/Si interface with the electron beam being aligned parallel to the Si [110] axis, exhibiting a clean and well-defined single crystal diffraction pattern serving as a strong indicator of the highly epitaxial nature of GeSn STIL on Si substrates. In this pattern, the separation of the diffraction spots from GeSn and Si was observed on (0 0 2l) (where $l = \pm 1, 2, 3, \ldots$) along the direction of film growth, as indicated by the arrow, but such separation was not observed on the (2h 2h 0) diffraction spots (where $h = \pm 1, 2, 3, \ldots$) along the interface. This indicates that the GeSn lattice is compressed along the interface plane to coherently join with that of Si without any mismatch. The lattice mismatch along the growth direction is about 5.85%. EDS analysis from multiple locations showed that the GeSn STIL has a Sn content of 10–11 at. %.

Figures 4(c) and 4(d) exhibit a plan-view TEM image and one-quarter of a SAED pattern extracted from a plan-view GeSn STIL/Si interface with the electron beam parallel to the [001] Si. The GeSn STIL exhibits a continuous morphology over the 2D film plane. The SAED pattern showcases a clean single crystal diffraction pattern without any splitting of diffraction spots. Figure 4(e) shows a cross-sectional HRTEM image presenting an atomic structure of the GeSn STIL/Si interface. Misfit dislocations were rarely observed at the interface. However, nanotwins or stacking faults initiating at a height of ~2 nm above the interface were frequently observed, as denoted by arrows in Fig. 4(e). Figure 4(f) exhibits a plan-view HRTEM image of the GeSn STIL/Si taken with the electron beam aligned parallel to the Si [001] axis. This image presents a pattern similar to that of [001] Si in HRTEM, without the presence of 2D modulated superlattice arrangements.

It can be seen from the above results that the GeSn thin layers on (001) Si deposited at 457 and 313 °C encompass distinct film morphologies and composition. The GeSn STIL sample, deposited at a lower temperature, consists of a continuous 10 nm thick

27 March 2024 13:52:56

Published under an exclusive license by the AVS

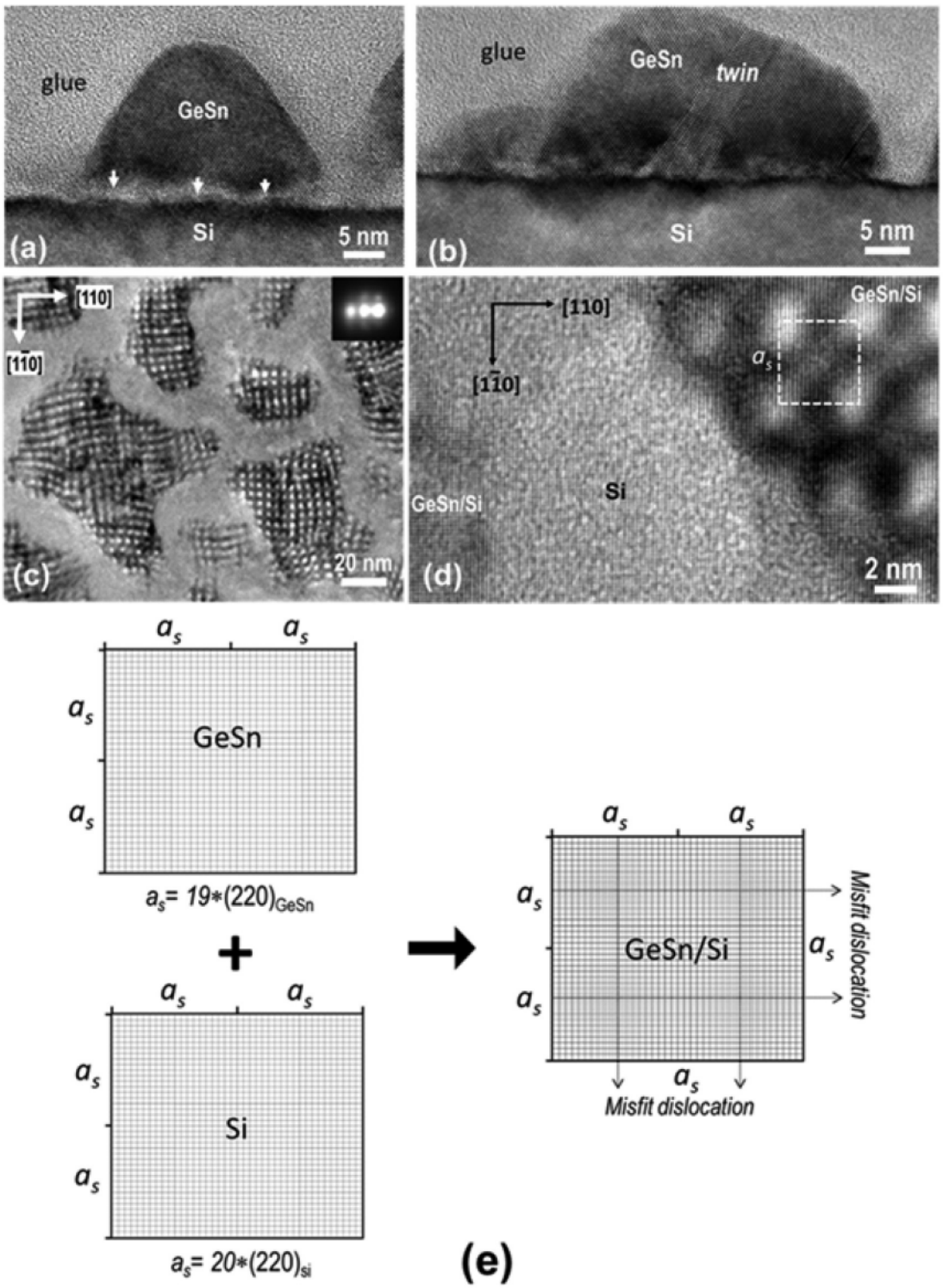

FIG. 3. (a) and (b) Cross-sectional HRTEM images of GeSn HTIL film on Si. (c) Plan-view TEM image and (d) plan-view HRTEM image of the GeSn HTIL/Si. (e) Illustration of the formation of 2D superlattice at the GeSn/Si interface. Arrows in (a) denote the locations of misfit dislocations.

27 March 2024 13:52:56

Published under an exclusive license by the AVS

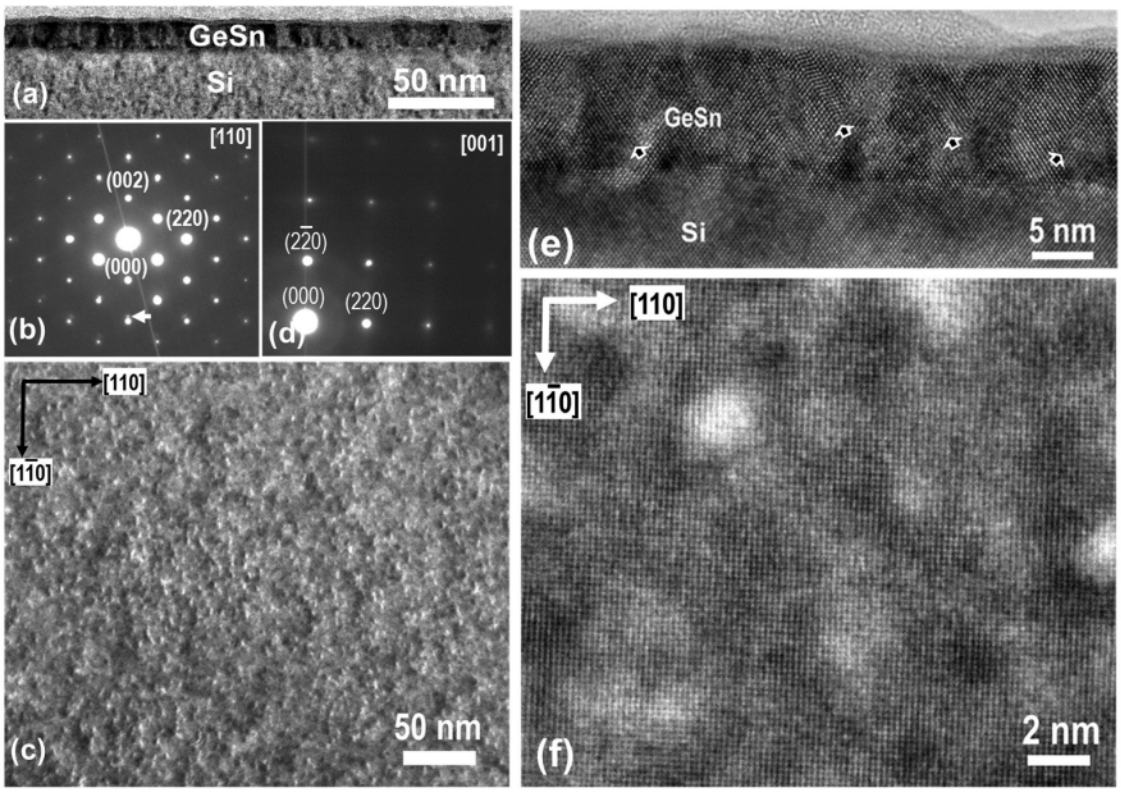

FIG. 4. (a) Cross-sectional TEM image and (b) SAED pattern of GeSn STIL film on Si substrates, (c) plan-view TEM image, and (d) one-quarter of a SAED pattern of the GeSn STIL film on Si. (e) Cross-sectional HRTEM image and (f) plan-view HRTEM image of GeSn STIL/Si.

27 March 2024 13:52:56

epilayer with 10%–11% Sn content. In contrast, the GeSn HTIL, deposited at a higher temperature, exhibits a discrete island morphology with a lower Sn content. These variations are mainly caused by the difference in atomic mobility on the surface at different deposition temperatures. At a lower temperature, reduced atom mobility limits the migration of Ge and Sn adatoms on the surface, possibly leading to a layer-by-layer growth mechanism for GeSn. This process retains Sn adatoms, resulting in a higher Sn content in the film. In this case, the GeSn lattice is compressed to coherently join that of Si in the film plane, forcing the lattice to expand along the growth direction and resulting in a larger lattice mismatch between GeSn and Si. The lattice misfit strain along the growth direction accumulates during the growth of the film and is relieved by the formation of nanotwins and stacking faults. The STIL displays a smooth surface, making it a potential template for growing multilayer or multi-quantum well structures.

For the GeSn film grown at a higher temperature, the mobility of the Ge and Sn adatoms is enhanced. The growth of the GeSn film could proceed according to the following scenario. The initial few monolayers of GeSn growth follow a 2D nucleation process, resulting in the formation of 2D plates on the surface of the (001) Si substrate. The lattice misfit strain between GeSn and Si can be relaxed through the formation of misfit dislocations at the interface resulting in a nonuniform stress distribution across the 2D GeSn plates. The edge regions of the 2D plates experience high levels of stress, while the top surfaces of the 2D plates exhibit lower stress. With further growth, the adatoms on the film surface will be transported from the stressed regions to the less stressed regions through a surface diffusion process. As a result, island-like structures are formed, as shown in Fig. 2(a) with a hemispherical shape to minimize surface energy. Enhanced atom mobility could lead to the simultaneous outward diffusion of Sn atoms from the stressed inner region to the less stressed surface. The surface region of the GeSn islands would then contain higher Sn content than the interior of the crystal. This seems to be in general agreement with the results obtained through XPS and EDS analysis (Table I).

Furthermore, in the case of smaller GeSn islands with an FWHM less than 20 nm, the stress generated within the structure during growth can easily travel toward the surface, resulting in a defect-free structure. Conversely, in larger islands with an FWHM exceeding 25 nm, the stress propagation path is insufficient to reach the surface, leading to the formation of nanotwins and/or stacking faults within the structure. It appears that the formation of a high-temperature initial layer with island-like morphology offers an effective means to accommodate the lattice misfit strain at the GeSn/Si interface, thereby significantly reducing residual strain

Published under an exclusive license by the AVS

TABLE I. Comparison of film morphology and defects, interface structure, lattice mismatch, Raman peak position, and Sn content obtained by different methods in GeSn HTIL and STIL films.

		HTIL at 457 °C	STIL at 313 °C
Film morphology		Isolated epitaxial islands	Continuous epilayer
Defects in film		No defect in smaller islands, nanotwins/stacking faults in larger islands	Nanotwins/stacking faults above the interface
Interface		Misfit dislocations	No misfit dislocations
Lattice mismatch		5.2% (interface plane) 4.7% (growth direction)	0 (interface plane) 5.8% (growth direction)
Raman peak position		296 cm^{-1}	291.5 cm^{-1}
Sn content	XPS	6.0 at. %	9.5 at. %
	Raman	6.5 at. %	12.5 at. %
	EDS	7–8 at. % (core) 9–10 at. % (near-surface)	10–11 at. %

within the GeSn epilayer. This is expected to confer favorable advantages for the production of thicker, high-quality epitaxial GeSn thin films.

IV. SUMMARY AND CONCLUSIONS

Ultra-thin GeSn HTIL and STIL deposited on (001) Si substrates using RPECVD produce epitaxial structures. The GeSn STIL has a thickness of ~10 nm, consisting of a continuous epitaxial layer with its lattices being compressed along the interface plane to coherently match Si. Mismatch dislocations were rarely formed at the interface but nanotwins or stacking faults initiated within the structure, above the interface. The GeSn HTIL film exhibits discrete epitaxial island morphology with a peak height of ~30 nm and an FWHM ranging from 20 to 100 nm. Misfit dislocations between the islands and the (001) Si substrate formed two-dimensional modulated superlattice structures at the interface plane. GeSn islands with an FWHM smaller than 20 nm are defect free whereas those beyond 25 nm contain nanotwins and/or stacking faults. The formation of a high-temperature initial layer with island-like morphology offers an effective means to accommodate the lattice misfit strain at the interface, thereby significantly reducing residual strain within the GeSn epilayer and is expected to confer favorable advantages for the production of thicker, high-quality epitaxial GeSn thin films directly on (001) Si substrates.

ACKNOWLEDGMENTS

This work was supported by the U.S. Air Force (Award No. FA8650-20-2-5853/Subaward No. SPC-1000006781|GR128665), AFOSR LRIR 19RYCOR032 (G. Pomrenke and W. Miller), and by the U.S. National Science Foundation under Award No. NSF/DMR 2122128.

AUTHOR DECLARATIONS

Conflict of Interest

The authors have no conflicts to disclose.

Author Contributions

Jiechao Jiang: Conceptualization (equal); Data curation (equal); Formal analysis (equal); Funding acquisition (equal); Investigation (equal); Methodology (equal); Project administration (equal); Resources (equal); Supervision (equal); Validation (equal); Visualization (equal); Writing – original draft (equal); Writing – review & editing (equal). **Nonso Martin Chetuya:** Conceptualization (equal); Data curation (equal); Formal analysis (equal); Investigation (equal); Methodology (equal); Visualization (equal); Writing – original draft (equal); Writing – review & editing (equal). **Efstathios I. Meletis:** Conceptualization (equal); Formal analysis (equal); Funding acquisition (equal); Investigation (equal); Methodology (equal); Project administration (equal); Resources (equal); Supervision (equal); Validation (equal); Writing – original draft (equal); Writing – review & editing (equal). **Joseph H. Ngai:** Conceptualization (equal); Formal analysis (equal); Funding acquisition (equal); Investigation (equal); Methodology (equal); Project administration (equal); Resources (equal); Supervision (equal); Visualization (equal); Writing – original draft (equal); Writing – review & editing (equal). **Gordon J. Grzybowski:** Conceptualization (equal); Formal analysis (equal); Funding acquisition (equal); Investigation (equal); Methodology (equal); Project administration (equal); Resources (equal); Supervision (equal); Visualization (equal); Writing – original draft (equal); Writing – review & editing (equal). **Bruce Claflin:** Conceptualization (equal); Formal analysis (equal); Funding acquisition (equal); Investigation (equal); Methodology (equal); Project administration (equal); Resources (equal); Supervision (equal); Validation (equal); Visualization (equal); Writing – original draft (equal); Writing – review & editing (equal).

DATA AVAILABILITY

The data that support the findings of this study are available within the article.

REFERENCES

[1]J. Mathews, R. T. Beeler, J. Tolle, C. Xu, R. Roucka, J. Kouvetakis, and J. Menéndez, Appl. Phys. Lett. **97**, 221912 (2010).
[2]S. Gupta, B. Magyari-Köpe, Y. Nishi, and K. Saraswat, J. Appl. Phys. **113**, 073707 (2013).
[3]S. Wirths *et al.*, Nat. Photonics **9**, 88 (2015).
[4]S. Zaima, O. Nakatsuka, N. Taoka, M. Kurosawa, W. Takeuchi, and M. Sakashita, Sci. Technol. Adv. Mater. **16**, 043502 (2015).
[5]J. Chrétien *et al.*, ACS Photonics **6**, 2462 (2019).
[6]Y. Zhou *et al.*, ACS Photonics **6**, 1434 (2019).
[7]Y. Zhou *et al.*, Optica **7**, 924 (2020).
[8]R. Olesinski and G. Abbaschian, Bull. Alloy Phase Diagrams **5**, 265 (1984).
[9]G. Grzybowski, M. E. Ware, A. Kiefer, and B. Claflin, J. Vac. Sci. Technol. B **38**, 062209 (2020).
[10]B. Claflin, G. J. Grzybowski, M. E. Ware, S. Zollner, and A. M. Kiefer, Front. Mater. **7**, 44 (2020).
[11]S. Assali, J. Nicolas, and O. Moutanabbir, J. Appl. Phys. **125**, 025304 (2019).
[12]W. Dou *et al.*, Sci. Rep. **8**, 5640 (2018).

27 March 2024 13:52:56

Published under an exclusive license by the AVS

[13]J. Segura-Ruiz *et al.*, Mater. Sci. Eng., B **264**, 114899 (2021).
[14]H. Stanchu, A. V. Kuchuk, Y. I. Mazur, J. Margetis, J. Tolle, J. Richter, S. Yu, and G. J. Salamo, Semicond. Sci. Technol. **35**, 075009 (2020).
[15]Y. Miao *et al.*, Mater. Sci. Semicond. **85**, 134 (2018).
[16]V. R. D'Costa, J. Tolle, R. Roucka, C. D. Poweleit, J. Kouvetakis, and J. Menéndez, Solid State Commun. **144**, 240 (2007).
[17]J. C. Jiang, J. He, E. I. Meletis, J. Liu, Z. Yuan, and C. L. Chen, J. Nano Res. **3**, 59 (2008).
[18]J. C. Jiang, E. I. Meletis, Z. Yuan, and C. L. Chen, Appl. Phys. Lett. **90**, 051904 (2007).
[19]J. C. Jiang, J. He, E. I. Meletis, C. L. Chen, Y. Lin, J. Horwitz, and A. J. Jacobson, Thin Solid Films **518**, 147 (2009).

27 March 2024 13:52:56

Published under an exclusive license by the AVS